Journal of
Mechanical
Science and
Technology

Journal of Mechanical Science and Technology 21 (2007) 2091~2100

Assessment of floor response spectrum by parametric error estimation and its application to a spring-mounted reactor vessel assembly

Moon Shik Park*

Department of Mechanical Engineering, Hannam University, 133 Ojung-dong, Daeduk-gu, Daejon, Republic of Korea 306-791

(Manuscript Received February 6, 2007; Revised July 5, 2007; Accepted July 9, 2007)

Abstract

For large facilities having several floors or containers, floor response spectra, FRS, other than ground response spectra need to be developed. However, FRS can have error especially when components are not small in their masses. In this paper, error is estimated in order to specify applicability of the FRS by deriving and comparing with analytic results for two degrees of freedom system. An identity regarding modal vectors and participation factors in the modal method is used to measure the FRS error. It is found that FRS is sufficiently accurate if the mass of a component is one hundredth or less than that of the floor. On the contrary, it is shown that fixed frequency of a component does not affect the FRS accuracy considerably. A compact power plant system consists of two main assemblies with spring mounts is applied as an example for the derivation of the FRS and several aspects associated with its modeling and calculation are discussed.

Keywords: Ground response spectrum; Floor response spectrum; Reactor vessel assembly; Shock loading; Spring mounts; Finite element method

1. Introduction

Large facilities requiring both safety and function as major concerns need to be designed, built and maintained against any dynamic loads that may cause catastrophic consequences to the facilities, human and their environment. Regulations and design codes are demanding to design such facilities as nuclear power plant, transportation structure, multistory building, liquefied natural gas tanks and large scale pipelines with respect to earthquake events that may occur in very low probability.

Response spectrum analysis has been effectively used to analyze and design structures, buildings and vehicles for earthquake vibrations or other types of dynamic loads. Seismic engineering group use design response spectra as their primal earthquake loading. Structures may be modeled as elastic or inelastic according to the stress level of the materials. Diverse methods and trends in earthquake engineering societies can be found in the literatures [1-3]. Similar to response spectrum analysis in earthquake engineering, U.S. Navy developed Dynamic Design Analysis Method, DDAM, for the design of warships and underwater vehicles. DDAM is a design response spectrum developed by numerous underwater shock tests in relation to systems or equipments mounted on various locations of the ships. Extensive details about DDAM and its applications are found in Scavuzzo and Pusey [4] or more recently in Liang et al. [5]. Vehicles under certain impact also require design by appropriate shock response spectra e.g. spacecraft launcher in pyrotechnic shock [6], vessels impacting water [7] etc. More elaborate approaches to analyze such a system have been exploited by other researchers. They take not only disturbing sources but also transferring media into account the system that inevitably result in complex time integration of soil-structure [8, 9] or fluid-structure [10, 11] coupled

*Corresponding author. Tel.: +82 42 629 8278, Fax.: +82 42 629 8293
E-mail address: ms.park@hannam.ac.kr

problem.

FRS is outlined for example in IAEA [2] and it is very effective to design secondary systems or equipments. Modeling of main structure as well as ground excitation loads can be alleviated in the design of equipments if we use appropriate FRS. Deterministic and probabilistic methods of deriving FRS for a nuclear power plant can be found in Paskalov and Reese [12]. DDAM can also be considered as FRS for it specifies floors as deck, hull or shell plating. FRS can be derived from realistic ground motions in time history or simulated time history. A simulated or artificial time history can be obtained from a design response spectrum adopting its relations to the power spectral density functions, see e.g. Refs. [12, 13]. However FRS should be applied with care when the mass of a equipment is not sufficiently small comparing to that of the floor. It may also depend on the frequency ratio of equipment to floor. So those aspects need to be assessed before application.

This paper is first to assess error occurred in FRS by a simple two dof model. And the paper is deriving applicable FRS of a compact power plant system consisting of two heavy structures and soft spring mounts between them

2. Power plant system characterization

The model to examine this study is a compact power plant system consists of two heavy structures and arrays of springs between these two main structures as shown in Fig. 1. RVA is a pressurized reactor vessel assembly which contains many primary and secondary systems which are fair amount of efforts-taking components to design. IST is an isolation structural tank with built-in walls of metal inside and it is filled with water. The concept of springs here is to absorb any severe dynamic load exerted by the ground so that the RVA should perform their desired functions in a safe manner. Mounting location of the springs is determined as indicated in Fig. 1 rather than at the bottom of the IST. It is to avoid becoming excessively large springs in case of supporting both of two heavy masses. Therefore a load path concept from the ground to the RVA components is through the IST, springs, reactor vessel and then to the components. The notion of component will be used here without particular indication whether it is actually a part, an assembly or a subsystem.

To characterize the system dynamically, it is neces

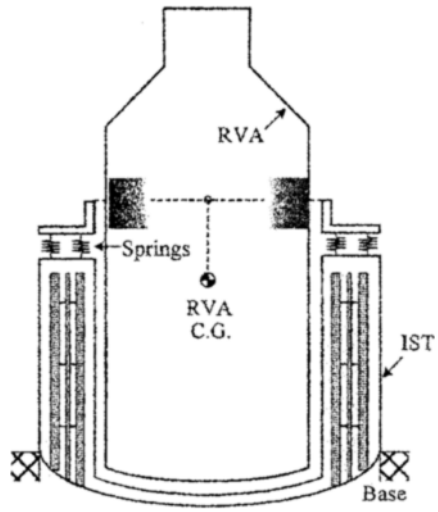

Fig. 1. The RVA supported by the springs and the IST.

sary to classify ranges of mass, stiffness, degree of damping and their natural frequencies. Overall weights are 170 tons and 210 tons for the RVA and the IST, respectively. Other ranges including geometric dimensions are outlined in Table 1. The reactor vessel can be considered as rigid in this study comparing to the stiffness of the IST and the springs. The springs supporting the RVA may have very low natural frequencies on the other hand the IST itself has wide range of low and high natural frequencies because of the shell nature of the structure. So the system can be characterized as in Fig. 2 where Ω_1 and Ω_2 represent fixed natural frequencies of the IST and the RVA-springs, respectively and ω_i represents natural frequency of the typical component. M_2 means mass of the RVA while K_2, C_2 represent stiffness and damping coefficients of the springs. M_1, K_1 and C_1 mean mass, stiffness and damping coefficient of the IST although C_1 can be regarded as zero if there is no significant structural damping or viscous damping within the IST. Finally m_i represents the mass of a component.

It is very effective and advantageous to use FRS for the design of components within the RVA because it can eliminate the need of modeling all the RVA, the springs and the IST which are quite complex and time consuming. However, assessment of the accuracy according to the respective ratios of masses and frequencies need to be done before using FRS. So this study will investigate two major concerns arising from questions like how accurate is FRS and how is it affected by the IST. Dynamic responses of the RVA

with respect to the IST are investigated first and then FRS for the components with respect to the RVA are investigated by using the system of Fig. 2.

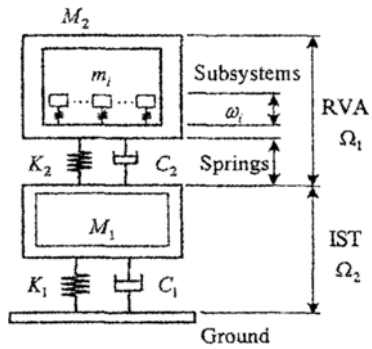

Fig. 2. Lumped characterization of the spring-mounted RVA system.

Table 1. Overall ranges of approximate properties and dimensions.

	IST	Springs	RVA	Individual Component
Weight	210 tons	1 ton	170 tons	under 1 ton
Fixed natural frequency	over 20 Hz	Under 10 Hz	(RVA +Springs)	vary
Size	Φ 4.7 m x 2.8 m (d x h)	133 mm (h)	Φ 2.7 m x 5.3 m (d x h)	vary

Note) d: outer diameter, h: overall height

3. Ground response spectrum

Ground response spectrum is a curve of spectral response against frequency for wide range of single dof oscillators excited by a particular ground motion. This term is used in contrast to floor response spectrum which will be described in section 5. Various types of sources and ground motions exist. Fig. 3 shows some types of ground motion in acceleration-time history. Whatever the excitation is, ground response spectrum can be obtained by transient analysis of the following single degree of freedom system with natural angular frequency of ω_n and damping ratio of ζ.

$$\ddot{z} + 2\zeta\omega_n \dot{z} + \omega_n^2 z = -\ddot{x}_0 \tag{1}$$

where, $z = x - x_0$ is a relative displacement between the oscillator motion x and the ground motion x_0. Integration of Eq. (1) is performed either by direct integration or by Duhamel's integration [14]. Using the solution of Eq. (1), oscillator's acceleration is recovered by

$$\ddot{x} = -\omega_n^2 z - 2\zeta\omega_n \dot{z} \tag{2}$$

and it's spectral acceleration is obtained as

$$S_a = \ddot{x}_{\max} = \max_t(\ddot{x}(t)) \tag{3}$$

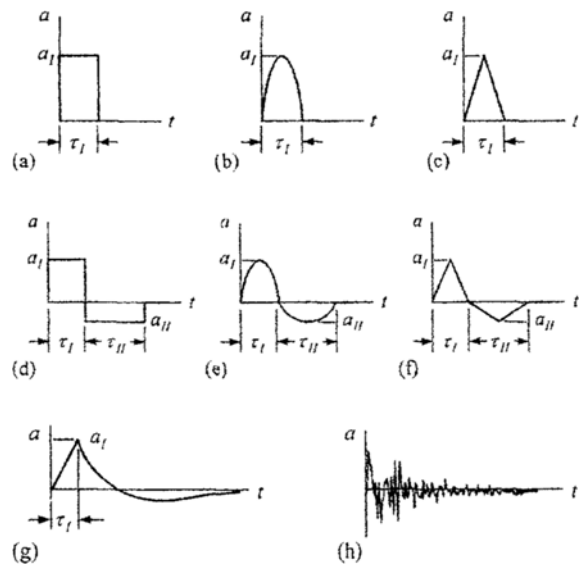

Fig. 3. Various types of ground excitations in acceleration-time history. (a), (b) and (c) single rectangle, half sine and triangle pulse, (d), (e) and (f) double rectangle, half sine and triangle pulse, (g) linear exponential type, (h) complex type.

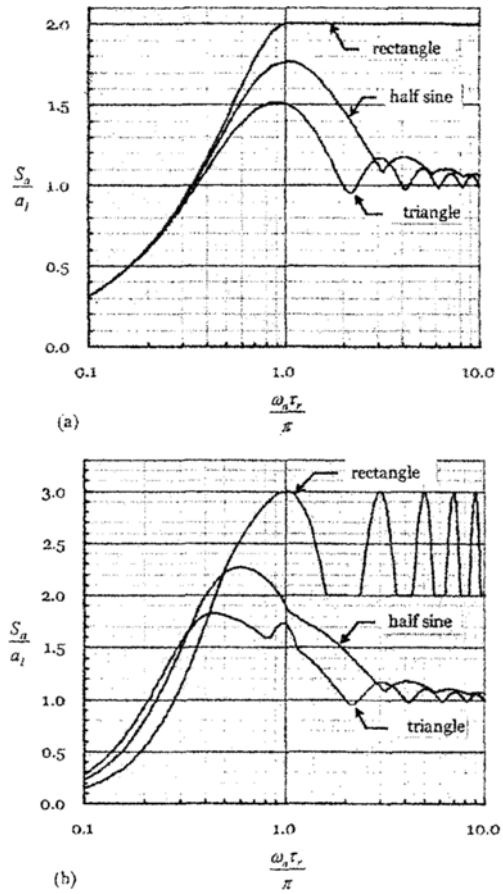

Fig. 4. GRS for typical (a) single pulse excitations and (b) double pulse excitations.

Typical ground response spectra are calculated by using NASTRAN [15] and shown in Fig. 4(a) for excitations of Figs. 3(a), (b) and (c) and in Fig. 4(b) for excitations of Figs. 3(d), (e) and (f), respectively. No damping is considered in deriving Fig. 4. Abscissa in the figures is taken non-dimensional so that it can be interpreted as either a response spectrum or a spectrum for varying periods of excitation. In case of double pulse excitations of Fig. 3, a_I and a_{II} are the magnitudes of acceleration and the condition $a_I\tau_I = a_{II}\tau_{II}$ is imposed with the value of $a_{II}/a_I = 0.5$ so that ground motion remains stationary at the end of excitation. Time period τ_r is to make the value of $a_I\tau_r$ is equal to the area of the first pulse in acceleration time history that is $\tau_r = \tau_I$ for rectangle, $\tau_r = \tau_I/2$ for triangle and $\tau_r = 2\tau_I/\pi$ for half sine, respectively. It is observed that the maximum spectrum value occurs around frequency of $f_n = \omega_n/2\pi = 1/2\tau_r$ in Fig. 4(a) while it occurs at distant

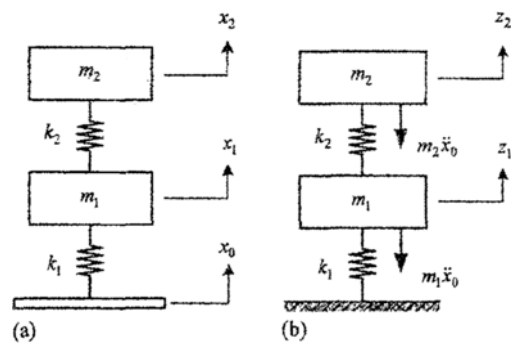

Fig. 5. Equivalence of two dof system under ground excitation (a) ground excited system (b) fixed and equivalently forced system.

frequencies in Fig. 4(b). As a matter of fact, these spectra represent envelope of primary and residual spectra. See Harris and Piersol [6] for other types of excitations and their response spectra. Practical design response spectra for any complex excitation including earthquake or shock should be constructed based upon ground response spectra with factors involving site and probabilistic nature of excitation. Those are not of concern of this study.

4. Response spectrum of two degrees of freedom system

Taking account dynamic design requirements of the RVA described in the previous section as well as the load path characteristics as in Fig. 2, it is necessary to evaluate effects of the IST to the dynamic behavior of the RVA with respect to the springs. The RVA and the IST have same order of heavy masses comparing to their components as listed in Table 1. Therefore it can be described by 2 dof system as shown in Fig. 5(a) where 1 and 2 means the IST and the RVA, respectively and damping is not shown for simplicity but it can be considered straight forward. Note that the springs are three dimensional and the IST has many degrees of freedom but only the first mode of the vertical direction will be considered in this paper. Some higher modes of the IST vibration may cause dynamic amplification to certain components in the RVA when they have similar frequencies but it will be considered in the later section.

Dynamic equation of a vibratory multi-dof system exerted by the external force $\{F\}$ is:

$$[m]\{\ddot{x}\} + [k]\{x\} = \{F\} \tag{4}$$

When the system is excited by the ground displacement x_0, equivalent to Eq. (4) can be written as:

$$[m]\{\ddot{z}\}+[k]\{z\}=-[m]\{1\}\,\ddot{x}_0 \tag{5}$$

where, $\{z\}=\{x\}-\{1\}\,x_0$ is a vector of relative displacement and $\{1\}$ is a vector of unit elements. Eq. (5) can be represented as Fig. 5(b) that is equivalent to Fig. 5(a) in two dof system. In Eqs. (4) and (5), $[m]$ is a mass matrix and $[k]$ is a stiffness matrix such that:

$$[m]=\begin{bmatrix} m_1 & 0 \\ 0 & m_2 \end{bmatrix};\ [k]=\begin{bmatrix} k_1+k_2 & -k_2 \\ -k_2 & k_2 \end{bmatrix} \tag{6}$$

To derive natural frequencies, either eigenvalue analysis or finding zeros of the determinant equation $\Delta=\det\left([k]-\omega^2[m]\right)$ can be used. Determinant of the two dof system Eq. (5) is:

$$\Delta=(k_1+k_2-\omega^2 m_1)(k_2-\omega^2 m_2)-k_2^2 \tag{7}$$

If we rewriting Eq. (7) by fixed natural angular frequencies as $\Omega_1=\sqrt{k_1/m_1}$, $\Omega_2=\sqrt{k_2/m_2}$, and by introducing a stiffness ratio $\kappa=k_2/k_1$, then zero of Eq. (7) is:

$$\tilde{\Delta}=\frac{\Delta}{k_1 k_2}=(1+\kappa-\frac{\omega^2}{\Omega_1^2})(1-\frac{\omega^2}{\Omega_2^2})-\kappa=0 \tag{8}$$

Introducing non-dimensional ratios $\Lambda=\omega^2/\Omega_1\Omega_2$, $\mu=m_2/m_1$ leads the solution of Eq. (8) to:

$$\Lambda^2-2\beta\Lambda+1=0 \tag{9a}$$

with

$$\beta=\frac{1}{2}\left[\sqrt{\kappa/\mu}+(1+\kappa)\sqrt{\mu/\kappa}\right] \tag{9b}$$

$$\Lambda_{1,2}=\beta\pm\sqrt{\beta^2-1} \tag{9c}$$

So, the natural angular frequencies are found by $\omega_{1,2}=\sqrt{\Omega_1\Omega_2\Lambda_{1,2}}$ and their results are plotted in Fig. 6 in case of $\mu=1$. It is observed from similar parametric study that two natural frequencies fall within ±2 % range of their fixed natural frequencies when $\Omega_2/\Omega_1<1/5$. Here, ±2 % can be considered as a design significance level which indicates that the natural frequencies are nearly the same as their fixed natural frequencies. Note that $\Omega_2/\Omega_1=\sqrt{\kappa}$ when $\mu=1$.

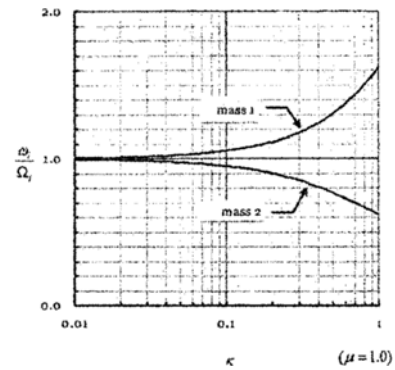

Fig. 6. Natural frequency ratios with respect to the stiffness ratios.

To derive response spectra for two dof system of Fig. 5, it is necessary to integrate Eq. (5) and this study uses modal method. Physical displacement $\{z\}$ is superposed by modal displacements q_a such that $\{z\}=\sum_a\{\phi_a\}\,q_a$. With natural angular frequency ω_a and its mode shape $\{\phi_a\}$ associated with mode a, Eq. (5) can be transformed into the following decoupled equations:

$$\ddot{q}_a+\omega_a^2 q_a=-P_a\ddot{x}_0(t) \tag{10a}$$

with

$$P_a=\frac{\{\phi_a\}^T[m]\ \{1\}}{\{\phi_a\}^T[m]\ \{\phi_a\}} \tag{10b}$$

Here, P_a is called by a participation factor of mode a. Solution of Eq. (10a) is a following Duhamel integral:

$$q_a=-\frac{P_a}{\omega_a}\int_0^t \ddot{x}_0(\xi)\ \sin\omega_a(t-\xi)\ \ d\xi \tag{11}$$

from Eq. (10a) and with the identity of $\sum_a\{\phi_a\}P_a=\{1\}$ [4]:

$$\begin{aligned}\{\ddot{x}\}&=\{\ddot{z}\}+\{1\}\ddot{x}_0=\sum_a\{\phi_a\}\ \ddot{q}_a+\{1\}\ddot{x}_0\\&=\sum_a\{\phi_a\}(-P_a\ddot{x}_0-\omega_a^2 q_a)+\{1\}\ddot{x}_0=-\sum_a\{\phi_a\}\omega_a^2 q_a\end{aligned} \tag{12}$$

Response spectrum can be constructed by evaluating Eq. (12) as in Eq. (3):

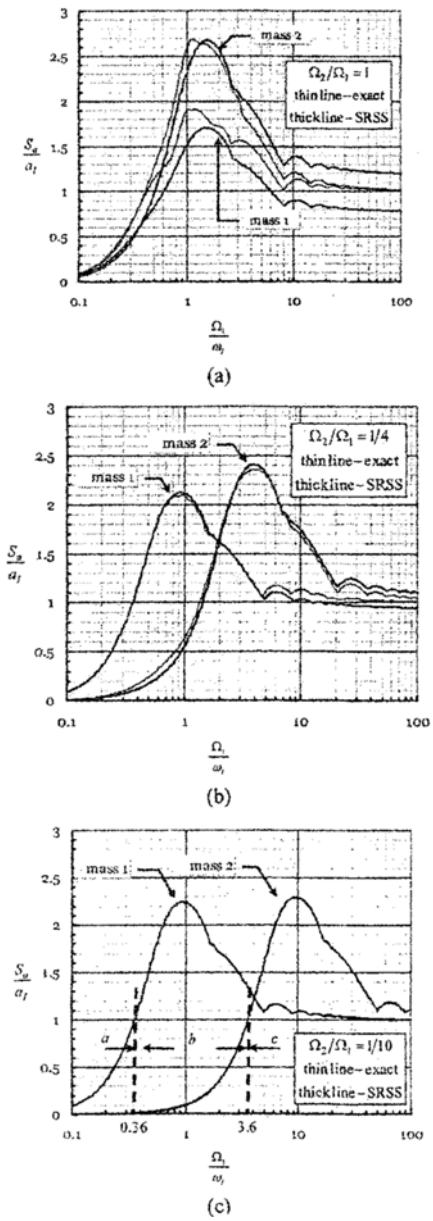

Fig. 7. Response spectra for two dof system having equal masses (a) $\Omega_2/\Omega_1 = 1$ (b) $\Omega_2/\Omega_1 = 1/4$ (c) $\Omega_2/\Omega_1 = 1/10$.

$$S_{a\ i} = \ddot{x}_{i\ \max} = \max_t \left[-\sum_a \phi_{a\,i}\, \omega_a^2\, q_a(t) \right] \tag{13}$$

However maximum responses in response spectrum analysis method are approximated without integrating Eq. (11) but by one of several approximate methods to Eq. (13) such as:

$$\ddot{x}_{i\ \mathrm{SRSS}} = \sqrt{\sum_a \left(\phi_{a\,i}\, P_a\, S_a \right)^2} \tag{14a}$$

Table 2. Modal analysis values and their SRSS magnitudes for two dof system.

$\frac{\Omega_2}{\Omega_1}$	$\frac{\omega_1}{\Omega_1}$	$\frac{\omega_2}{\Omega_2}$	$\{\phi_1\}$	$\{\phi_2\}$	P_1	P_2	$\|R_1\|_{\mathrm{SRSS}}$	$\|R_2\|_{\mathrm{SRSS}}$
1	1.6180	0.6180	0.8507 -0.5257	-0.5257 -0.8507	0.3249	-1.3764	0.7746	1.1832
1/4	1.0327	0.9684	0.9981 -0.0621	-0.0621 -0.9981	0.9359	-1.0602	0.9364	1.0598
1/10	1.005	0.9950	1.0000 -0.0100	-0.0100 -1.0000	0.9900	-1.0099	0.9900	1.0099

with known ground response spectra S_a as in Fig. 4 which means the value of:

$$S_a = \max_t \left[\omega_a \int_0^t \ddot{x}_0(\xi)\ \sin\omega_a(t-\xi)\ d\xi \right] \tag{14b}$$

where SRSS is one of norms which means square root of sum of squares. Other norms common in use are ABS, CQC and NRL [4].

Analytic solution of Eq. (11) for the double half sine excitation of Fig. 3(e) can be derived by adopting the following formula [6]:

$$\begin{aligned} \Psi_a(t,\omega) &= P_a \omega_a \int_0^t \sin\omega\xi \cdot \sin\omega_a(t-\xi) d\xi \\ &= \frac{P_a\ \omega_a^2}{\omega^2 - \omega_a^2} \left[\frac{\omega}{\omega_a} \sin\omega_a t - \sin\omega t \right] \end{aligned} \tag{15}$$

in which Ψ_a is a Duhamel integral of sine excitation function, $\sin\omega t$, for a particular mode a in terms of acceleration. Finally $\ddot{q}_a$ becomes:

$$\ddot{q}_a(t) = \begin{cases} a_I\ \ \Psi_a(t,\omega_I), & \text{if } t \le \tau_I \\ a_I\ \ \Psi_a(t,\omega_I) + a_I\ \ \Psi_a(t-\tau_I,\omega_I) & \\ \quad + a_{II}\ \ \Psi_a(t-\tau_I,\omega_{II}), & \text{if } \tau_I < t \le \tau_I + \tau_{II} \\ a_I\ \ \Psi_a(t,\omega_I) + a_I\ \ \Psi_a(t-\tau_I,\omega_I) & \\ \quad + a_{II}\ \ \Psi_a(t-\tau_I,\omega_{II}) + a_{II}\ \ \Psi_a(t-\tau_I-\tau_{II},\omega_{II}), & \\ \qquad\qquad \text{if } \tau_I + \tau_{II} < t \end{cases} \tag{16}$$

Using Eqs. (15) and (16), analytic calculation of transient response Eq. (12) and spectral response Eq. (13) are straight forward. Note that in the above equations, $\omega_I = \pi/\tau_I$ and $\omega_{II} = \pi/\tau_{II}$, respectively. Results of Eqs. (13) and (14a) for the two dof system of equal masses, $\mu = 1$, are drawn in Fig. 7 for several ratios of Ω_2/Ω_1 .

By observing Fig. 7, it is evident that the smaller the value of Ω_2/Ω_1 the closer the values of $\ddot{x}_{i\,\mathrm{SRSS}}$ in Eq. (14a) to the values of $\ddot{x}_{i\,\max}$ in Eq. (13). Some modal analysis values for this problem are listed in Table 2 where $\|R_i\|_{\mathrm{SRSS}} = \sqrt{\sum_a \left(\phi_{a\,i}\ P_a\right)^2}$ is a measure of accuracy of SRSS norm to compare with the following identity [4]:

$$\sum_a \phi_{a\,i} P_a = 1 \tag{17}$$

Note that $\ddot{x}_{i\,\mathrm{SRSS}} = \|R_i\|_{\mathrm{SRSS}}$ and $\ddot{x}_{i\,\max} = \sum \phi_{a\,i} P_a$ as $\omega_a/\omega_i \to \infty$. Comparing values of $\|R_i\|_{\mathrm{SRSS}}^{a}$ to Eq. (17) for various ratios of Ω_2/Ω_1, they are within $\pm 2\,\%$ closeness each other for about $\Omega_2/\Omega_1 < 1/8$. It can be justified that response spectra for two dof system can be derived approximately from those of GRS such as Fig. 4 with certain amount of errors.

Returning to the design problem in section 2, there may be three distinct design ranges *a*, *b* and *c* as shown in Fig. 7(c) which suggest different dynamic considerations required according the values of Ω_1/ω_i. If the value of Ω_1/ω_I is less than 0.36 that means excitation period is considerably shorter than the natural period of the IST, neither the IST nor the RVA shows dynamic amplification. If design is within the range *b* ($0.36 < \Omega_1/\omega_I < 3.6$), only the IST shows dynamic amplification. For design range *c* ($3.6 < \Omega_1/\omega_I$) that means excitation last quite long time comparing with the natural period of the IST, only the RVA shows dynamic amplification while the IST is moving almost rigidly with the ground.

5. Floor response spectrum and its error estimation

FRS is understood as a response spectrum measured on the floor of a multi-story building under certain ground excitation as shown in Fig. 8(a). Once FRS is available, it can be used to design equipments on that floor without consideration of the overall building and the nature of the excitation. Recalling the analyses in the previous section, the system of Fig. 1 can be further simplified as Fig. 8(b) which is a two dof problem consists of the RVA and a component of small mass. Applicability and accuracy of FRS in view of ranges of frequency and mass ratios will be assessed in this section by analyzing the simple system Fig. 8(b). A great deal of detailed FRS for the compact power plant system of Fig. 1 will be presented in the next section.

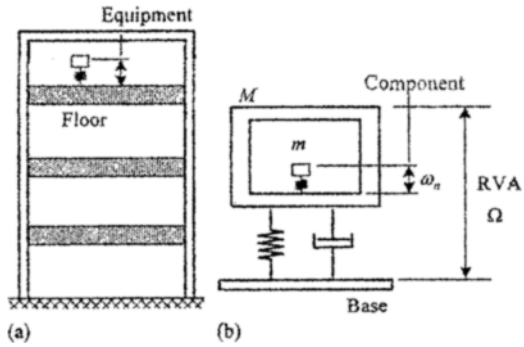

Fig. 8. Schematic representation of FRS (a) a multi-story building (b) the RVA and its components.

All the equations and the procedure in the previous section can be applied in the same manner with notions of M and m as the masses, Ω and ω_n as the fixed natural frequencies of the RVA and a component, respectively. Results for the double half sine ground excitation of Fig. 3(e) are plotted in Fig. 9. FRS curves for several frequency ratios of Ω/ω_I are shown in Fig. 9(a) in parallel with the GRS where $\omega_I = \pi/\tau_I$ and $\omega_n = \sqrt{k/m}$. Small amount of 2 % damping is applied for both the RVA and oscillators. In Fig. 9(a), FRS shows peak responses where oscillator's natural frequencies are close to that of the floor. It means there are frequency regions of oscillators, ω_n, that shall vibrate more severely than their floor and there is a possibility of severe oscillator vibration in case of $\omega_n \cong \Omega$. Dotted line in Fig. 9(a) indicate GRS of the floor and their corresponding FRS when $\omega_n/\omega_I \to \infty$. Fig. 9(b) shows exact spectral curves by analyzing oscillators as two dof system by Eq. (13) so that we can evaluate errors incurred by the FRS for $\Omega/\omega_I = 1/5$ and various values of $\mu = m/M$. From Fig. 9(b), it can be seen that there is very little difference between exact and FRS curves for very small values of μ. To estimate errors, FRS values may be compared with exact spectral values with respect to frequency and mass ratios as $\omega_n/\omega_I \to \infty$ where the oscillator should vibrate rigidly with the floor. Extensive analyses are done and the results are summarized by Table 3. As separated by dotted lines in Table 3, errors incurred by the FRS are within $\pm 1\,\%$ for small values of $\mu \le 1/100$ no matter what the frequency ratio, Ω/ω_I, is. Recalling the fact that most of components, equipments or subsystems in the RVA are much smaller than $\mu = 1/100$, applicability of the FRS can be justified by the Table 3.

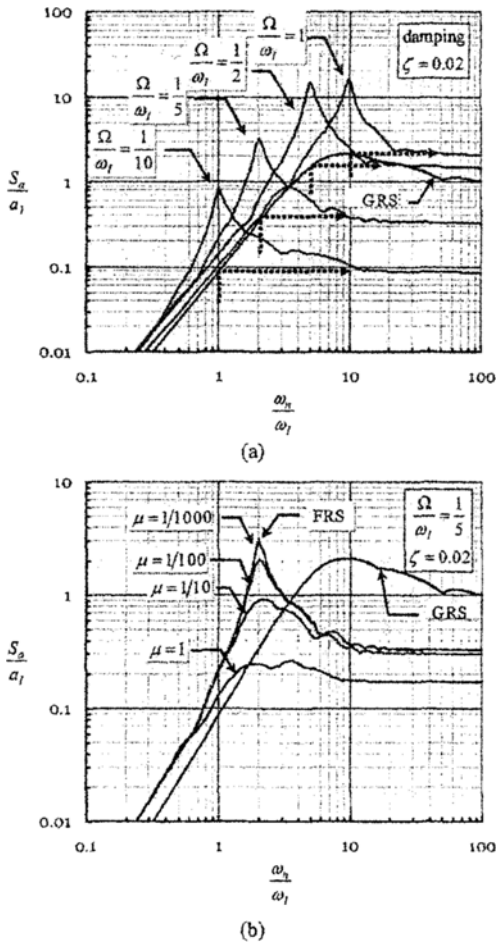

Fig. 9. Response spectra of two dof system having various mass and frequency ratios. (a) FRS for varying frequency ratios (b) comparison FRS with exact values for varying mass ratios.

Table 3. Values of *(FRS-Exact)/FRS* as $\omega_n/\omega_l \to \infty$ for various frequency and mass ratios.

$\frac{\Omega}{\omega_l}$	mass ratios ($\mu = m/M$)				*FRS*
	1/1000	1/100	1/10	1	
1/10	0.002	0.010	0.090	0.497	0.087
1/5	0.001	0.010	0.086	0.485	0.334
1/2	-0.001	0.004	0.056	0.390	1.500
1	-0.008	-0.008	-0.009	0.054	2.108

6. Application for the spring-mounted RVA system

As explained in the section 2, appropriate springs are to be mounted on the top plate of the IST structure to support the RVA in conjunction with a skirt structure and to isolate dynamic loads at the same time. One of the helical wire rope springs is selected as a result of design trade-offs coping with static and dynamic design considerations as well as built and maintenance aspects. The springs and their arrangements are shown in Fig. 10(a) where directional naming conventions of the springs are shown also. Total of 108 springs are used such that 36 springs are located along inside while 72 springs are located outside to avoid any interference among them.

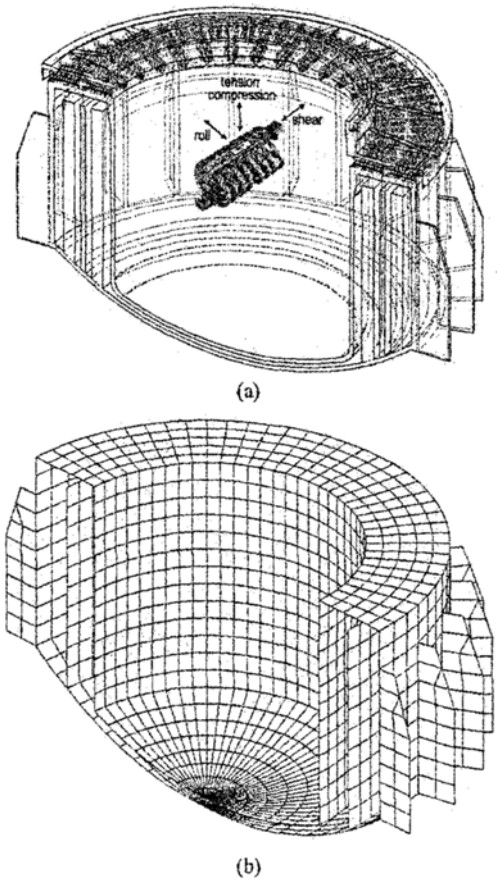

Fig. 10. Section view of the IST. (a) solid model and direction convention of the springs. (b) finite element model (springs, rigid bars, mass elements not shown).

The spring is made of many twisted strands of high strength steel wires and coiled to form helical turns so that it can resist to heavy loads in either of three directions or in arbitrary direction. The spring shows apparent damping due to inter strand dry friction and its value is catalogued as approximately 10 to 20 % equivalent viscous damping. Nonlinear force-deflection curves are plotted as in Fig. 11 according to the manufacturer's data where data points are

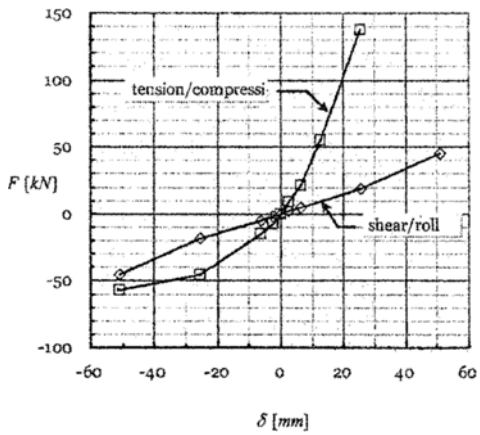

Fig. 11. Directional nonlinear load-deflection curves of the spring.

shown by the marks in the figure. Tension stiffness is higher than that of compression while shear and roll stiffness are the same each other and symmetric. In this study, dissipation is always considered to be 10 % equivalent to viscous damping which is regarded conservative as a design standpoint.

The FRS at the center of gravity of the RVA is calculated in this section. According to the discussions and analyses done in the section 4, the IST must be accounted for in the calculation of FRS. FRS will be a representation of dynamic load to the components within the RVA although the IST is not necessary to compute the dynamic response of the RVA. The IST is modeled by 4,440 quadrilateral and 168 triangular shell finite elements by NASTRAN as in Fig. 10(b). Each spring is modeled by three CBUSH1D elements along each orthogonal direction to cater for nonlinearities of Fig. 11 and its damping. The RVA is modeled by a rigid body having mass and moments of inertia linked with the springs by rigid bar elements. Ground motions in horizontal or vertical plane are applied through nodes at the corner of bottom shell and outer cylinder shell. Only vertical direction is explained in this paper to exemplify the application of the study.

Spring deflection for the RVA weight is calculated as 6.67 mm by nonlinear static analysis. Starting at such a deflected state, maximum and minimum relative deflection of the RVA by dynamic load is calculated as 19.5 mm in compression and 16.3 mm in tension, respectively. Results of the RVA acceleration shown in Fig. 12 are calculated by nonlinear dynamic analysis. Normal mode analysis can be done if the

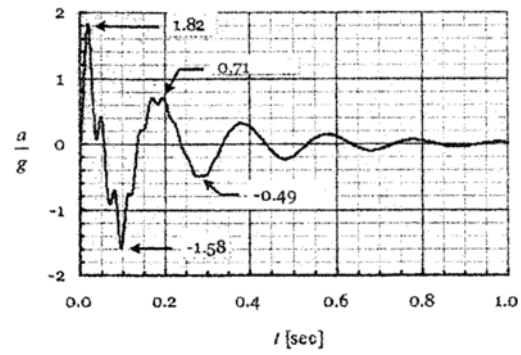

Fig. 12. Acceleration response at C.G. of the RVA.

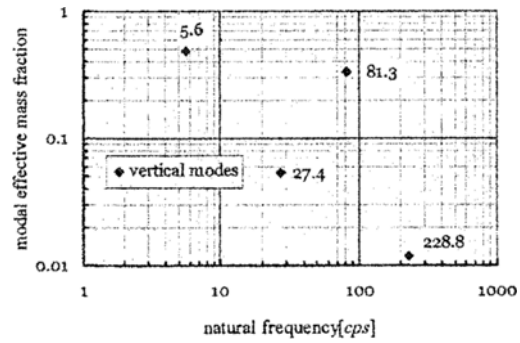

Fig. 13. Natural frequencies and their modal effective mass fractions.

spring coefficient of Fig. 11 are linearized such that spring stroke between up and down is regarded by a secant stiffness. Using such stiffness of 2058 Nmm^{-1} for each spring, natural frequencies, mode shapes, modal participation factors and modal effective masses and their fractions are calculated and displayed as in Fig. 13. Effective modal mass M_a is one that causes inertial force onto the ground by a mode as $F_a = M_a S_a$ from Scavuzzo and Pusey [4]:

Looking upon the vertical direction shown in Fig. 13, significant modes are those of 5.6, 27.4, 81.3 Hz whose mode shapes are vertical vibration of the springs, the inner cylinder shell and the bottom shell of the IST, respectively. Such modes contribute to the dynamic behaviors by some degree and can be seen by Fig. 12 as high frequency harmonics. The FRS is calculated and plotted in Fig. 14 by using acceleration of Fig. 12. In the figure, the input GRS is shown as well and FRS's for several damping ratios are plotted. The FRS shows two peaks in their spectral values which can be interpreted as vibration of the spring around 6 Hz and vibration of inner cylinder shell of

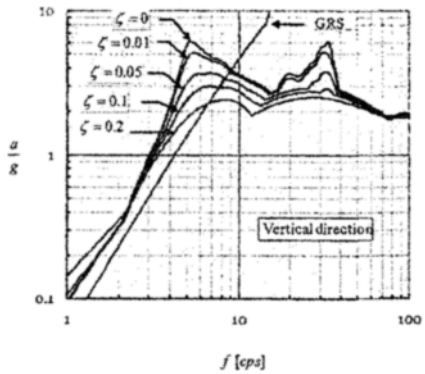

Fig. 14. FRS of the RVA-springs-IST system in vertical direction.

the IST around 30 Hz that was identified by a modal analysis. The later mode can only be accounted for if the IST is modeled appropriately and that is the reason why the IST should be modeled in the calculation of the FRS. This fact is important for the design of components because the spectrum can reach over $6\,g$ for natural frequency about 30 Hz even though the RVA is vibrating in acceleration less than $2\,g$.

7. Conclusions

Ground response spectra for some single and double pulse excitations are calculated. Transient dynamic response equations are derived analytically for two degrees of freedom problem under the double half sine pulse ground excitation. Analytic solutions are used to calculate exact response spectra and the exact spectra are compared to the FRS so that errors are estimated at various ranges of frequency and mass ratios. It can be concluded that the FRS is very close to the exact one when the mass of the component is sufficiently small comparing to that of the floor, i.e. $\mu \leq 1/100$ relatively regardless of the frequency ratios. As an application of the study, the compact power plant system having the IST, the RVA and the nonlinear springs was modeled, analyzed and evaluated to derive the FRS on the center of gravity of the RVA. It was found that some local vibration modes in the IST may increase the FRS severely so the IST needed to be modeled to calculate appropriate FRS. Those FRS can be used to design and analyze components, equipments and subsystems in the RVA.

Acknowledgement

This paper is funded by the research grant of Hannam University 2006.

References

[1] M. Saatcioglu and J. Humar, Dynamic analysis of buildings for earthquake-resistant design, *Canadian Journal of Civil Engineering* 30(2) (2003) 338-359.

[2] IAEA, Earthquake experience and seismic qualification by indirect methods in nuclear installations, IAEA-TECDOC-1333 IAEA Vienna (2003).

[3] U.S. Army Corps of Engineers, Engineering and design - seismic design provisions for roller compacted concrete dams, EP 1110-2-12 Department of the Army Washington D.C. (1995).

[4] R. J. Scavuzzo and H. C. Pusey, Naval shock analysis and design, SAVIAC Falls Church VA. (2000).

[5] C. C. Liang, Yang and M. F. Yuh-Shiou Tai, Prediction of shock response for a quadrupodmast using response spectrum analysis method, Ocean Engineering 29 (2002) 887-914.

[6] [6] C. M. Harris and A. G.. Piersol, Harris' shock and vibration handbook, Fifth Ed. McGraww-Hill New York (2002).

[7] A. Carcaterra, E. Ciappi, A. Iafrati and E. F. Campana, Shock spectral analysis of elastic systems impacting on the water surface, *Journal of Sound and Vibration* 229(3) (2000) 579-605.

[8] J. P. Wolf, Soil-structure interaction analysis in the time domain, Prentice Hall, Englewood Cliffs New Jersey (1988).

[9] A. M. Chandler, N. T. K. Lam and M. N. Sheikh, Response spectrum predictions for potential near-field and far-field earthquakes affecting Hong Kong: soil sites, *Soil Dynamics and Earthquake Engineering* 22 (2002) 419–440.

[10] T. L. Geers and B. A. Lewis, Doubly asymptotic approximations for transient elastodynamics, *Int. J. Solids Structures* 34(11) (1997) 1293-1305.

[11] D. Ranlet and R. P. Daddazio, A submerged shock response problem suitable for use as a benchmark, Proceedings of the 68th Shock and Vibration Symposium (1997) 96-104.

[12] A. Paskalov and S. Reese, Deterministic and probabilistic floor response spectra, *Soil Dynamics and Earthquake Engineering* 23 (2003) 605-618.

[13] N. C. Nigham and S. Narayanan, Application of random vibrations, Addison-Wesley Singapore (1994).

[14] D. J. Inman, Engineering vibration, Prentice Hall New Jersey (2001).

[15] NASTRAN Finite element analysis system, Quick Reference Guide MSC Software Corporation (2002).